Food & Function

Accepted Manuscript

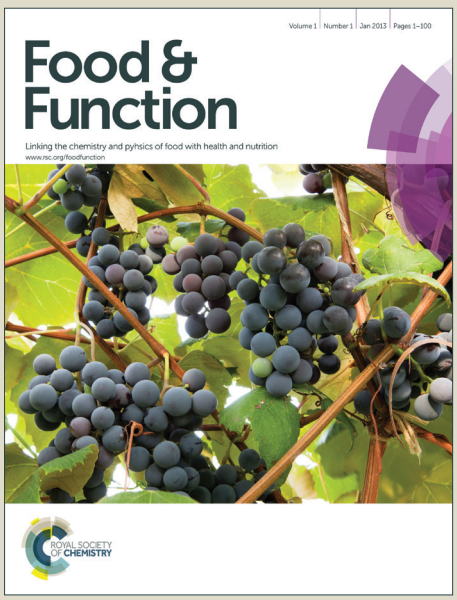

This is an *Accepted Manuscript*, which has been through the Royal Society of Chemistry peer review process and has been accepted for publication.

Accepted Manuscripts are published online shortly after acceptance, before technical editing, formatting and proof reading. Using this free service, authors can make their results available to the community, in citable form, before we publish the edited article. We will replace this *Accepted Manuscript* with the edited and formatted *Advance Article* as soon as it is available.

You can find more information about *Accepted Manuscripts* in the Information for Authors.

Please note that technical editing may introduce minor changes to the text and/or graphics, which may alter content. The journal's standard Terms & Conditions and the Ethical guidelines still apply. In no event shall the Royal Society of Chemistry be held responsible for any errors or omissions in this *Accepted Manuscript* or any consequences arising from the use of any information it contains.

ROYAL SOCIETY OF CHEMISTRY

www.rsc.org/foodfunction

Propagating longitudinal contractions in the ileum of the rabbit - efficiency of advective mixing†

Luke Fullard,*[a] Willem Lammers,[b] Graeme C. Wake,[c] and Maria J. Ferrua [d]

Received Xth XXXXXXXXXX 20XX, Accepted Xth XXXXXXXXX 20XX
First published on the web Xth XXXXXXXXXX 200X
DOI: 10.1039/b000000x

Three longitudinal motions of the rabbit small intestine were modelled in the CFD software Polyflow using *ex-vivo* experimental data previously reported in literature. Consideration was given to chyme rheology and mixing performance of the macro-scale lumenal motions, as triggered by the observed wall motions. Simulations were performed to qualitatively assess the flow behaviour. The advective properties of the flow were universally characterised by analysing the stretching ability of the flow. Two Newtonian fluids, with viscosities of $\mu = 1Pa.s$ and $\mu = 0.001Pa.s$, and a non-Newtonian shear-thinning fluid (Bird-Carreau relationship with $n = 0.41$, $\lambda = 0.1$, $\eta_\infty = 5.01 \times 10^{-9} Pa.s$ and $\eta_0 = 0.65Pa.s$) were investigated. It was found that both the type of contraction and chyme rheology significantly affected the flow and subsequent efficiency of advective motions in the intestinal core. Results also showed that shear rates generated were too small to unveil the pseudo-plastic behaviour of the non-Newtonian fluid. Of the longitudinal motions analysed, the oral propagation was the one leading to the higher, but also the most localised levels of stretching in the rabbit small intestine. This oral propagation was largely characterised by an ordered axial flow and was able to facilitate mixing by stretching material elements in the vicinity of the intestinal wall, particularly in the case of a low viscous water like fluid.

1 Introduction.

The dynamic motions of the small intestine in the mammalian gastrointestinal tract are wonderfully complex. There exist multiple regimes of intestinal muscular motion which differ with species, diet, prandial or postprandial period, and gut health, to name a few[1–3]. These movements are controlled anatomically by the intestinal twin muscular layer; an outer layer of axially directed cells which generally act to lengthen or shorten the intestine, and an inner circular layer which generally alters the diameter of the intestine[4]. Historically, motions of the small intestine have been divided into three general groups; peristalsis, segmentation, and longitudinal motions[4,5]. Within each of these three groups there are sub-motions which can themselves be classified according to their motion or genesis, such as in Lammers (2005)[6]. The study of segmental and peristaltic motions is more advanced than the study of longitudinal motions[7]. It is generally thought that segmentations result from contractions of the circular muscle layer, while peristaltic motions are a result of the combined contraction of both major muscle layers[1]. Longitudinal motions (sometimes called sleeve contractions or pendular motions) are less studied, however, have been of increased interest in recent years[2,3,5–9]. This type of motion is thought to be mostly caused by the contraction and relaxation of the longitudinal muscle layer[1]. The flow and mixing response of intestinal digesta to longitudinal wall motions is experimentally difficult to assess, yet has significance to our understanding of the digestive process.

In particular, propagating longitudinal contractions were found to be spatially and temporally coupled to the intestinal slow wave pacemaker in the rabbit intestine[6]. It was concluded that motions are determined by both the origin of the slow wave and the direction of propagation of the slow wave. Motion was always in the opposite direction to slow wave transit. That is, if the slow wave moved orally, the motion of the intestine was aborally, and vice versa. Additionally, the propagating longitudinal motions observed in the rabbit intestine[6] were organised into four categories. We consider three of these categories in the current paper; an oral motion (associated with an aborally moving slow wave), a compression (associated with two slow waves moving in opposite directions away from a single point, also known as a slow wave pacemaker site), and a stretching motion (associated with a colli-

† Electronic Supplementary Information (ESI) available: [details of any supplementary information available should be included here]. See DOI: 10.1039/b000000x/

[a] *Address, Institute of Fundamental Sciences, Massey University, Palmerston North, New Zealand; E-mail: L.Fullard@Massey.ac.nz*
[b] *Address, Department of Physiology, College of Medicine and Health Sciences, United Arab Emirates University, United Arab Emirates; E-mail: wlammers@smoothmap.org*
[c] *Address, Institute of Natural and Mathematical Sciences, Massey University, Auckland, New Zealand; E-mail: G.C.Wake@Massey.ac.nz*
[d] *Address, The Riddet Institute, Massey University, Palmerston North, New Zealand; E-mail: M.Ferrua@Massey.ac.nz*

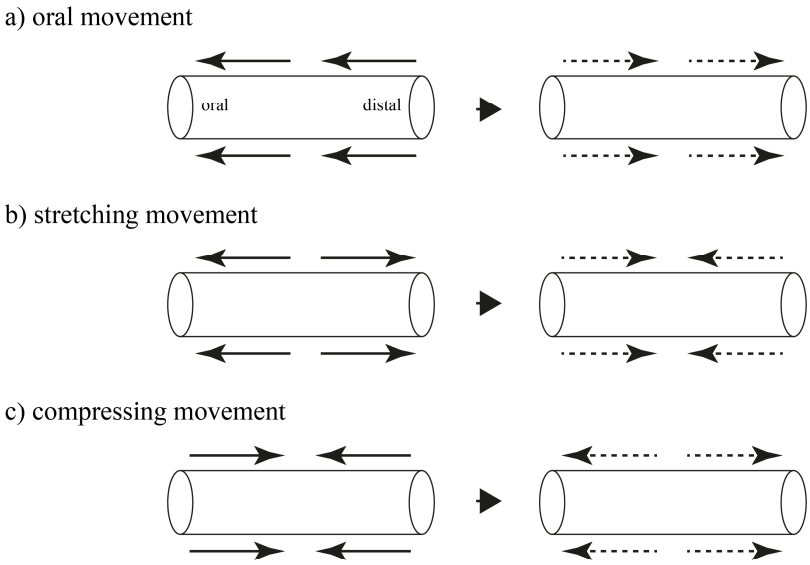

Fig. 1 Visual description of the three motions considered in this study.

sion of two slow waves). We do not consider an aboral motion here, since we expect this to be fluid dynamically similar to an oral motion. The oral motion observed by Lammers[6] can be considered almost unidirectional. Since one side of the intestine moves before the other (due to the slow wave propagation from oral to aboral) there is some visible lengthening of the intestinal wall which will affect flow dynamics. The stretching motion involves two sides of the intestine pulling away from each other. The compressive motion results in two sides of the intestinal wall moving towards each other, see Figure 1. By conservation of mass, we expect these types of motion to promote radial flow within the lumenal region. Videos of the experimentally observed motions are available on YouTube[10].

Two main functions of the contractions of the small intestine are to mix and propel the contained digesta. It has been suggested that longitudinal motions of the small intestine do not contribute significantly to transport through the intestine, but rather, may enhance mixing and absorption of nutrients[2,8]. Here, we consider how propagating longitudinal motions affect the dynamics and advective properties of the digesta in the lumen of the intestine. The fluid-mechanical function of greatly simplified longitudinal contractions was studied mathematically and experimentally by Melville et al. (1975)[7]. The first study to use CFD concepts to describe fluid motions and mixing in the intestine due to longitudinal muscle activity was de Loubens et al. (2013)[8]. Real wall motions of the proximal duodenum of rats and guinea pigs were recorded, analysed, and fed into a lattice-Boltzmann numerical code which, in turn, predicted the resulting motion of the chyme. It was concluded that pendular activity facilitates diffusive mixing within viscous fluids and acts to accelerate mass transfer over the boundary of the lumen of the intestine. The motions described by Lammers[6] differ from those used by de Loubens[8], likely due to the differing animal on which experiments were performed. The rheology of the intestinal digesta is of importance when analysing the mixing dynamics of intestinal contents as a result of intestinal motility. The fluid flow triggered by longitudinal motions was found to be weakly dependent on viscosity, when the chyme is modelled as a Newtonian fluid[8].

The objective of this study was to analyse behaviour and advective properties of the bulk motions generated in the rabbit small intestine by the three propagating longitudinal motions described by Lammers (2005)[6]. We are primarily interested in macroscopic (i.e. in the bulk of the organ) effects and we neglect micro-scale contributions such as movement of the villi lining the intestinal wall. The contribution of villi motility has been recently investigated by Lentle et al.[11] and Wang et al.[12]. In particular, by using a simplified model of the macro-scale lumenal motions Wang et al.[12] showed that

> In the absence of outer macro-scale eddies, the MML (micro-mixing layer) is far less effective in

enhancing absorption, while the enhancement of absorption by the MML in the presence of macro-scale transport is quite significant.

Therefore, the purpose of this work is to quantify the advective properties of macro-scale motions caused by propagating longitudinal contractions as a proxy to describe enhanced mixing and absorption of intestinal contents during digestion. Of interest was how digesta of different rheological properties respond to the observed wall motions. As in de Loubens et al. (2013)[8] we study two Newtonian fluids, but additionally analyse a non-Newtonian shear-thinning fluid. Unlike previous studies, the ability of longitudinal motions to promote mixing within the intestine was investigated and universally quantified by measuring their ability to continuously stretch and fold differential fluid elements within the domain.

CFD simulation software (ANSYS Polyflow) has been used to provide a numerical approach to investigate flows and mixing in the intestine for this complex flow problem.

2 Methods.

The work outlined in this paper comprises three parts; review of the experimental results of Lammers[6], inputting the resulting wall motions into Polyflow and outputting the flow behaviour, and analysis of advective mixing calculated in a Polyflow post-processor.

2.1 Intestinal geometry.

To reduce the computational cost of the simulation the section of intestine was modelled as an axisymmetric tube. In accordance with the experimental procedure of Lammers[6], the inner diameter of the intestinal segment was modelled as $4.5mm$, the length of the segment was modelled as $35mm$. The intestinal wall thickness was modelled as $0.5mm$. This geometry was meshed using the in built ANSYS meshing tool to produce a mesh with 1728 nodes and an average quality (a measure of suitability of the mesh where values close to 1 indicate a good mesh) of 0.977. As the simulation progressed the mesh was adapted automatically as necessary.

2.2 Intestinal motility.

Lammers[6] tracked the motility pattern of the rabbit ileum by recording the location of soot markers during longitudinal motion of the intestinal segment. Each soot marker was visually tracked to give time-dependent displacements using a custom software SmoothMap. It is the displacement of these soot markers which allow us to characterise the motion of the intestinal wall and to simulate the longitudinal motion using ANSYS Polyflow. We assume that the displacements of the soot markers were representative of the revolution of intestine at a given horizontal position. It is noted that the three types of motion of interest had differing amplitudes of displacement of the soot markers. The stretching and compressive motions were found to have relatively small displacement amplitudes when compared with the oral motion. The positions of the soot markers were measured from the video recording and found to be spaced at intervals (beginning at one end of the intestinal segment) $5.6mm$, $1.8mm$, $2.8mm$, $4.4mm$, $3.6mm$, $3.5mm$, $4.5mm$, $3.7mm$, and $5mm$. The location of each of these points at different instants of time was imported into Polyflow to impose horizontal displacement at points in our numerical simulation. The sections of intestine between these points are allowed to deform naturally via a fluid solid interaction. The vertical displacement of the wall is also allowed to deform in a similar way. Again, there were three types of motion simulated in this study; an oral motion, a stretching, and a compression. The motion was not modified when the rheology of intestine contents ware changed. This assumption may be justified by the findings of Lentle et al. (2007)[13], who found little difference in motility with changing chyme viscosity.

2.3 Numerical model.

The laminar flow of incompressible intestinal contents was modelled by Equations 1 - 2.

$$\frac{\partial u_i}{\partial x_i} = 0, \tag{1}$$

$$\rho\left(\frac{\partial u_i}{\partial t} + u_j\frac{\partial u_i}{\partial x_j}\right) = \frac{\partial \tau_{ij}}{\partial x_j} - \frac{\partial P}{\partial x_i}. \tag{2}$$

Equations 1 and 2 express the conservation of mass and momentum where, u_i, ρ, t, x_i, τ_{ij}, and P are the i'th component of velocity, the density, time, i'th component of the coordinate, the ij'th component of the fluid stress tensor, and the fluid pressure respectively. The choice of rheology determines the form of the stress tensor. For a Newtonian fluid, the stress tensor is assumed to be proportional to rate of strain, S_{ij}, with the viscosity, μ, as the constant of proportionality, as in Equation 3.

$$\tau_{ij} = 2\mu S_{ij}. \tag{3}$$

Some rheologies, such as the Bird-Carreau law model, may be considered generalised Newtonian fluids since they have a similar form to Equation 3, but their apparent viscosity, η, is dependent on the shear rate of the flow, $\dot{\gamma}$, as in Equation 4.

$$\tau_{ij} = 2\eta\left(\dot{\gamma}\right)S_{ij}. \tag{4}$$

For a Bird-Carreau fluid the apparent viscosity is given by

$$\eta = \eta_\infty + (\eta_0 - \eta_\infty)\left(1+\lambda^2\dot{\gamma}^2\right)^{\frac{n-1}{2}}, \tag{5}$$

Table 1 Rheology of intestinal chyme

Type	μ (Pa.s)	n	λ	η_∞ (Pa.s)	η_0 (Pa.s)	Similar to
Newtonian	1	-	-	-	-	Honey
Newtonian	0.001	-	-	-	-	Water
Bird-Carreau	-	0.41	0.1	5.01×10^{-9}	0.65	$5.5 g/L$ Guar gum

where η_∞ is the infinite-shear viscosity, η_0 is the zero-shear viscosity, λ is the natural time, and n is the power law index. Table 1 summarises the relevant parameters used in the model. The density of all three fluids in Table 1 is taken to be constant, $\rho = 1000 kgm^{-3}$. Gravity is neglected in this work hence it is omitted in the momentum equation. We also assume that the flow is driven by the wall motion.

At the interface between the fluid and the walls of the intestine we allow a fluid-solid interaction where the wall can deform elastically under stress and impact of the flow, and the fluid may have some impartation of momentum from the moving wall. The governing equation for the displacement of the elastic wall is given in the Polyflow user manual as

$$\nabla \cdot \sigma + \mathbf{f} = 0, \tag{6}$$

where σ is the elastic stress tensor and $\mathbf{f}$ is the body force. ANSYS Polyflow neglects transient terms in the elasticity equation. Assuming small deformations of the wall at successive time steps, the stress tensor in Equation 6 is given by

$$\sigma = \frac{E}{1+\nu}\left(\frac{\nu}{1-2\nu}\,\mathrm{tr}(\varepsilon)I + \varepsilon\right). \tag{7}$$

Here E and ν are elastic properties of the solid (the Young's modulus and the Poisson ratio) and ε is the strain tensor that relates to the wall displacement $\mathbf{d}$ as follows,

$$\varepsilon = \frac{1}{2}\left(\nabla \mathbf{d} + (\nabla \mathbf{d})^T\right). \tag{8}$$

When the wall is deformed, either by force exerted on the wall by a fluid, or by the imposed wall motion, the coordinates for the elastic domain are modified (after each time step) by

$$\mathbf{X}_{new} = \mathbf{X}_{old} + \mathbf{d}. \tag{9}$$

Using the above equations the system was modelled including a two-way fluid-solid interaction between the intestinal walls and contents. Based on the forces exerted on the wall by the fluid flow and local deformations imposed from the *ex-vivo* data of intestinal motility, the wall displacement ($\mathbf{d}$) is computed using Equation 6 at each individual time step. The body force term in Equation 6 corresponds to the forces imposed by the dynamic behaviour of lumenal contents on the wall (as predicted from Equations 1 and 2). As the wall deforms, it imposes a force on the fluid domain. A force term is added to the fluid momentum equation (Equation 2) equal to the force required to satisfy the velocity condition for the flow. In this way, a two-way fluid-solid interaction is defined. This model is solved using the in-built Polyflow solvers.

The Young's modulus and Poisson ratio were required to naturally move the sections of intestine between the points of imposed deformation. The choice of these parameters is not straightforward. Literature values for the Young's modulus span multiple orders of magnitude, see Table 2. It also appears that the value of these parameters vary depending on species. Preliminary simulations (not discussed here) were performed to investigate how the wide range of mechanical parameters affected the deformation of the wall between markers. We chose the elastic parameters measured in Chai et al.[17] as $E = 0.3 \times 10^4 Pa$, and $\nu = 0.35$ as they gave the more visually compelling motion.s

Initially we assume that the fluid is at rest, $u = 0$ at $t = 0$. We also assume a no-slip condition at the boundary of the fluid and the intestinal wall. At this boundary, motion is allowed to develop naturally via the elasticity parameters and the fluid solid interaction. The geometry was treated as axisymmetric so at the center of the tube an axisymmetric boundary is imposed. At the two ends of the tubular domain open boundary conditions are imposed so that fluid may flow in and out depending only on the deformations of the intestinal wall and not on the presence of a particular pressure gradient across the system. The system of equations was solved using the in-built algorithms of Polyflow. Specifically, a predictor-corrector time-marching scheme was used. In this study we chose to use the implicit Euler method for the corrector part of the algorithm. This is a first order method in time but does not cause any oscillatory numerical instability. A constant time-step of $0.04s$ was used for the entire simulation which was chosen as a fair balance of accuracy (since the scheme is first order) and computation time, while still being small enough to capture the generic motion of the intestinal wall during each of the three motilities. It was found that the solution converged in less than 10 iterations per time step.

2.4 Analysis of mixing - stretching values.

From a fundamental classical mechanics viewpoint the efficiency of advective mixing is characterised by the amount

Table 2 Literature values of elastic parameters

Reference	Animal	Young's modulus $\times 10^4$ (Pa)	Poisson ratio
Zhao Et Al[14]	Guinea pig	0.015 - 0.15	-
Liao Et Al[15]	Rat	1.7 - 3.24	-
Ohayon[16]	Unknown	8 - 16	-
Chai Et Al[17]	Human	0.3	0.35
Velec Et Al[18]	Human	1	0.499
Hari Et Al[19]	Human	1000	0.48
Chen Et Al[20]	Generic muscle	0.1 - 5	0.45 - 0.49

of stretching that differential material elements experience within the domain, as they are transported and deformed by the flow. This kinematic lamellar model, developed by Ottino[21], effectively quantifies the ability of a flow to deform matter and to generate interface. Ottino[21] developed this model to unify the treatment of the mixing of fluids from a kinematic perspective. It can be demonstrated that the amount of stretching (λ) experienced by any differential material line dX with a unit orientation M seeded within the flow domain can be calculated from the deformation gradient to which that line is exposed as it is being advected by the flow (10).

$$\lambda(X,M,t) = \sqrt{M \cdot CM}. \tag{10}$$

Here C is the right Cauchy Green strain tensor and is a function of the deformation gradient (i.e. velocity gradient). Mathematically it is defined by

$$C = F^t F,\ C_{IJ} = \frac{\partial x_k}{\partial X_I}\frac{\partial x_k}{\partial X_J}. \tag{11}$$

With the goal of characterising the amount of stretching generated within the intestine 2000 line segments (with random initial positions and orientations) were seeded within the domain and their motions and stretching tracked during the entire simulation time. The results can then be averaged over the simulation domain and a mean stretching value can be calculated for the domain. ANSYS Polyflow has a built in post-processor, named Polystat, to evaluate this parameter over the whole flow domain.

3 Verification of numerical methodology

In order to validate that the numerical methodology implemented is accurate we construct an exact solution to a simplified yet similar flow problem.

Consider a fluid filled infinite axisymmetric cylindrical tube of radius a, with walls oscillating with frequency ω. The governing equation of motion in cylindrical coordinates is

$$\frac{\partial u}{\partial t} = \frac{1}{R}\frac{\partial}{\partial R}\left(R\frac{\partial u}{\partial R}\right), \tag{12}$$

where subscripts denote the partial derivative, $R = \dfrac{r}{\sqrt{\nu}}$, r is the radial coordinate measured from the center of the tube, and ν is the kinematic viscosity. The boundary conditions are given as

$$u(r=a,t) = -D\sin(\omega t), \tag{13}$$

$$u(r=0,t) \quad \text{is finite.} \tag{14}$$

Initially the fluid contained within the tube is stationary.

The solution to this problem can be found using Laplace transforms. Denoting $\bar{u}$ as the transformed velocity and s as the transform variable, we obtain

$$\frac{\partial^2 \bar{u}}{\partial R^2} + \frac{1}{R}\frac{\partial \bar{u}}{\partial R} = s\bar{u}.$$

If we were to multiply this equation by R^2 then it would be in the form of a standard Bessel equation with solution

$$\bar{u}(R,s) = AI_0(\sqrt{s}R) + BK_0(\sqrt{s}R),$$

where A and B are constants, I_0 and K_0 are the modified Bessel functions of the first and second kind respectively. Since our solution must be finite at $r = 0$, then we find $B = 0$.

The boundary condition 13 may also be transformed to become

$$\bar{u}\left(\frac{a}{\sqrt{\nu}},s\right) = \frac{-D\omega}{s^2+\omega^2} = AI_0\left(\sqrt{s}\frac{a}{\sqrt{\nu}}\right).$$

This condition allows us to find the constant A, and hence write

$$\bar{u}(R,s) = \frac{-D\omega}{s^2+\omega^2}\frac{I_0(\sqrt{s}R)}{I_0\left(\sqrt{s}\dfrac{a}{\sqrt{\nu}}\right)}.$$

Before inverting the Laplace transformation to find the solution in the time domain we define the following functions:

$$\bar{u} = \bar{F}(s)\bar{G}(s),$$

where

$$\bar{F}(s) = \frac{-D\omega s}{s^2+\omega^2}, \qquad \bar{G}(s) = \frac{I_0(\sqrt{s}R)}{sI_0\left(\sqrt{s}\frac{a}{\sqrt{\nu}}\right)}.$$

Taking the inverse transforms of these functions individually:

$$f(t) = \mathscr{L}^{-1}(\bar{F}(s)) = -D\omega\cos(\omega t),$$

$$g(t) = \mathscr{L}^{-1}(\bar{G}(s)) = 1 - 2\sum_{n=0}^{\infty} exp\left(\frac{-\lambda_n^2 t}{A^2}\right)\frac{J_0\left(\lambda_n\frac{R}{A}\right)}{\lambda_n J_1(\lambda_n)},$$

where J_0 and J_1 are the Bessel functions of the first kind of order zero and one respectively, $A = \frac{a}{\sqrt{\nu}}$, and λ_n are the roots of J_0, i.e. $J_0(\lambda_n) = 0$ for all n. By the convolution theorem,

$$u(r,t) = \int_0^t f(t-\tau)g(\tau)d\tau, = -D\omega\int_0^t \cos(\omega(t-\tau))C_1 d\tau,$$

where

$$C_1 = 1 - 2\sum_{n=0}^{\infty} exp\left(\frac{-\lambda_n^2\tau}{A^2}\right)\frac{J_0\left(\lambda_n\frac{R}{A}\right)}{\lambda_n J_1(\lambda_n)}.$$

This integral can be evaluated to find

$$u(r,t) = -D\sin(\omega t) - \frac{2\omega D a^2}{\nu}\sum_{n=0}^{\infty}\frac{J_0\left(\frac{\lambda_n r}{a}\right)}{\lambda_n J_1(\lambda_n)}C_2, \qquad (15)$$

where

$$C_2 = \left[\frac{\lambda_n^2\nu^2 exp\left(\frac{-\lambda_n^2\nu t}{a^2}\right) - a^2\omega\nu\sin(\omega t) - \lambda_n^2\nu^2\cos(\omega t)}{\lambda_n^4\nu^2 + a^4\omega^2}\right].$$

3.1 Comparison of exact and numerical trials.

The analytical solution given in Equation 15 is compared to a numerical solution which is solved using Polyflow. The experiment is performed for two fluids, a honey like substance with significant dynamic viscosity ($\approx 1\ Pa.s$), and a water like substance with low viscosity ($\approx 0.001\ Pa.s$). Both fluids are given a density of $1000\ kg/m^3$. The radius of the tube is taken as $a = 2.25\ mm$, the angular frequency of oscillation is taken as $\omega = \pi/2\ rad/s$, the amplitude of oscillation is $D = 9\pi/4\ mm$. the above values are chosen as an approximate representation of oral oscillations in the rabbit ileum. The solution is plotted at four points in the tube; $r/a = 0.9$, $r/a = 0.75$, $r/a = 0.5$, and $r/a = 0.25$. Figures 2 and 3 show the results of our numerical experiment.

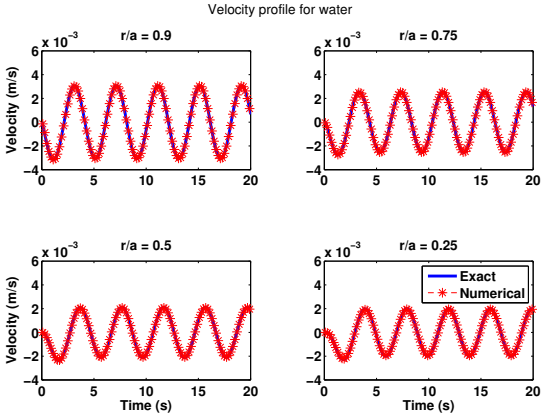

Fig. 2 Comparison of velocity predicted by the numerical scheme and the exact solution for water.

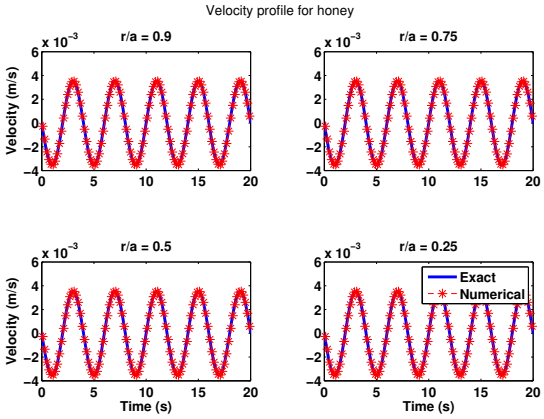

Fig. 3 Comparison of velocity predicted by the numerical scheme and the exact solution for Honey.

It may be noted that the numerical and exact solutions appear very similar. To quantify the error introduced by the numerical method we define the following error norm;

$$E = \frac{|\int u_{ex}dt| - |\int u_{num}dt|}{|\int u_{ex}dt|} \times 100, \qquad (16)$$

where E is the percentage error in the numerical solution, u_{ex} is the velocity obtained from the analytical solution, and u_{num} is the velocity obtained from Polyflow. In each case, the error was found to be less than 3.1%. This results leads us to have high confidence in our numerical solution.

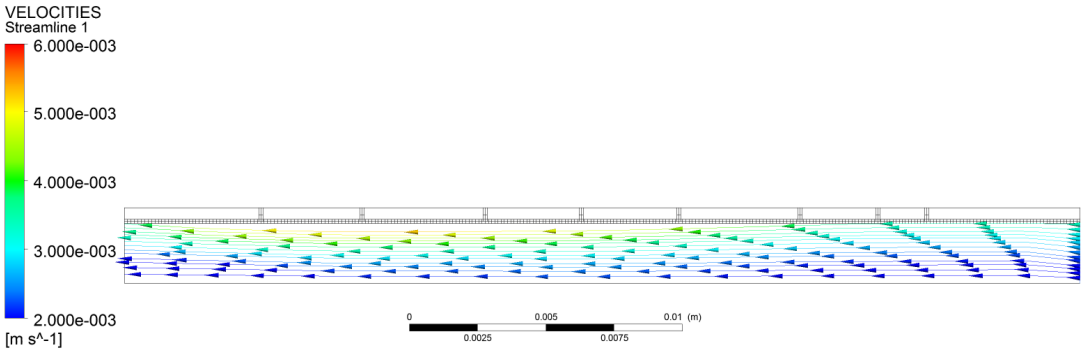

(a) Streamlines for water during an oral motion. Time 3*s*.

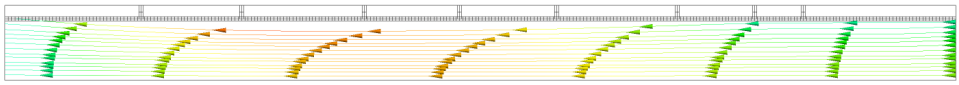

(b) Streamlines for honey during an oral motion. Time 3*s*.

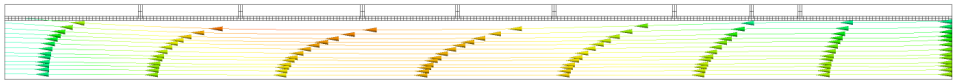

(c) Streamlines for Guar gum during an oral motion. Time 3*s*.

Fig. 4 Streamlines during an oral motion. Time 3*s*.

4 Results.

4.1 Oral motion.

Figure 4 contains plots of the instantaneous streamlines at time 3s, corresponding to the time of maximum displacement for the first observed oral movement of the wall in the intestinal segment. From top to bottom the contained fluids are (a) water, (b) honey, and (c) guar gum respectively. Regardless of fluid rheology, results indicate the development of a unidirectional axial flow within the lumen of the intestine. However, despite the similar behaviour of the flow, fluid rheology did have a profound effect on the distribution of flow properties and velocity profiles that develop within the intestine. As fluid viscosity increases, a more uniform velocity profile developed across the intestine, with the flow ultimately acquiring a plug-like behaviour for the high viscous Newtonian fluid. The Bird-Carreau fluid shows similar streamline behaviour to the case of honey during an oral propagation.

The figures in 5 are the shear rates observed during the motion at 3s for the three fluids. These figures are in good agreement with the behaviour of the flow previously discussed. The high shear rates always occurred closer to the intestinal wall and were significantly diminished by fluid viscosity. It is observed that the shear rates which develop during an oral wall motion are very similar for the high viscous Newtonian fluid and the Bird-Carreau. Due to the similar behaviour observed for the highly viscous fluid and the Bird-Carreau, the resulting apparent viscosity of the non-Newtonian fluid within the domain was investigated. As illustrated in Figure 6, the apparent viscosity does not change much from the zero shear viscosity, (i.e. $0.65 Pa.s$), with this fluid behaving much like a Newtonian fluid with constant viscosity. This result explains why the behaviour of the Bird-Carreau fluid is similar to that of honey, since the viscosity of honey and apparent viscosity of the guar gum are relatively close. This result has implications for flows of shear thinning/thickening fluids in the small intestine, as it appears that the rates of shear generated by longitudinal contractions are too weak to generate significant pseudo-plastic or dilatant viscous behaviour in the bulk flow of the small intestine.

4.2 Stretching motion.

Figure 7 shows the streamlines for our three fluid rheologies at 4s, the time of maximum displacement of the first experimentally observed stretching motion. Clearly in this case we see a large amount of recirculation in the flow, implying that fluid elements or particles entrained in the flow may move both axially and radially during flow. Again we note that, in general, the fluid velocities are higher in the higher viscous fluid. However, the velocities are much lower (including wall velocities)

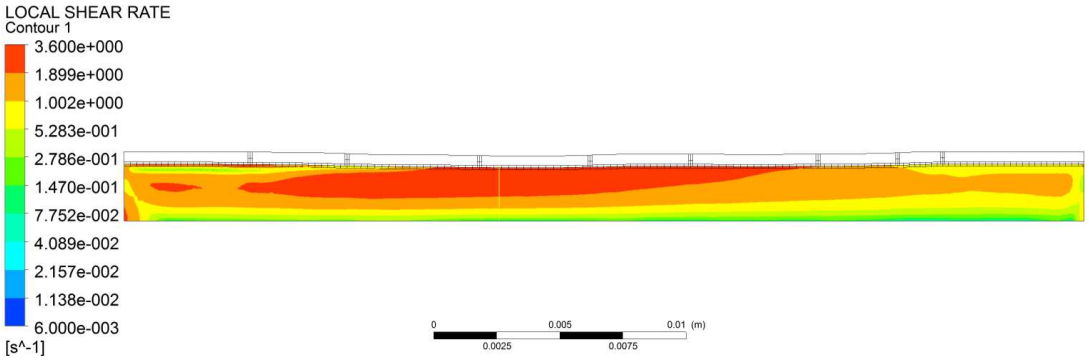

(a) Shear rate for water during an oral motion. Time 3*s*.

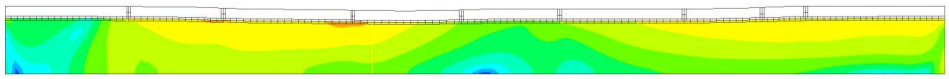

(b) Shear rate for honey during an oral motion. Time 3*s*.

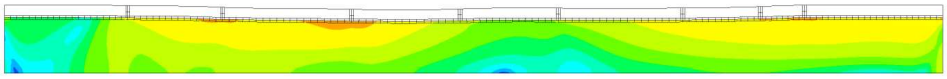

(c) Shear rate for guar gum during an oral motion. Time 3*s*.

Fig. 5 Shear rate during an oral motion. Time 3*s*.

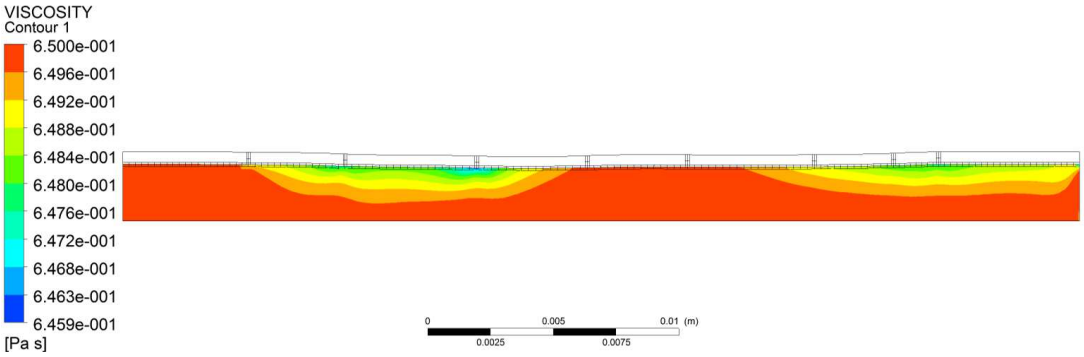

Fig. 6 Apparent viscosity of guar gum during an oral motion. Time 3*s*.

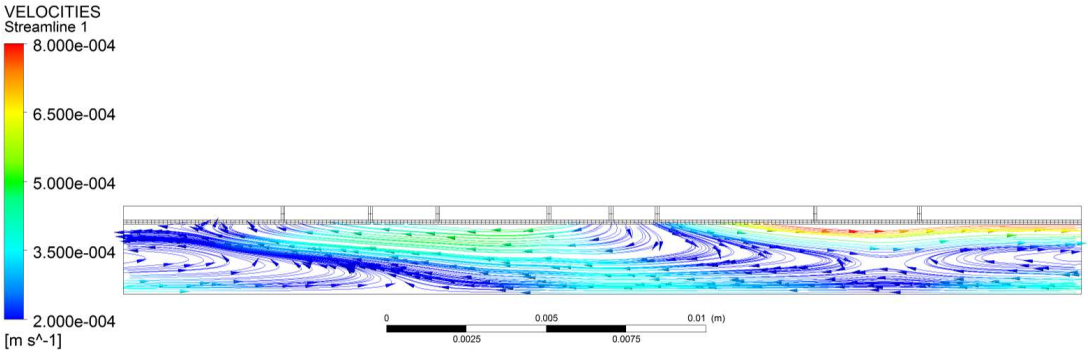

(a) Streamlines for water during a stretching motion. Time 4*s*.

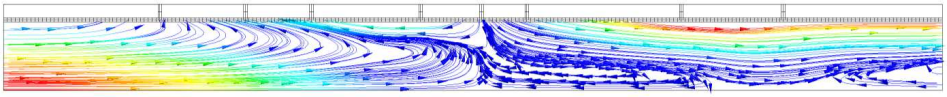

(b) Streamlines for honey during a stretching motion. Time 4*s*.

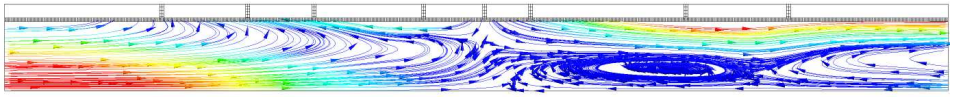

(c) Streamlines for guar gum during a stretching motion. Time 4*s*.

Fig. 7 Streamlines during a stretching motion. Time 4*s*.

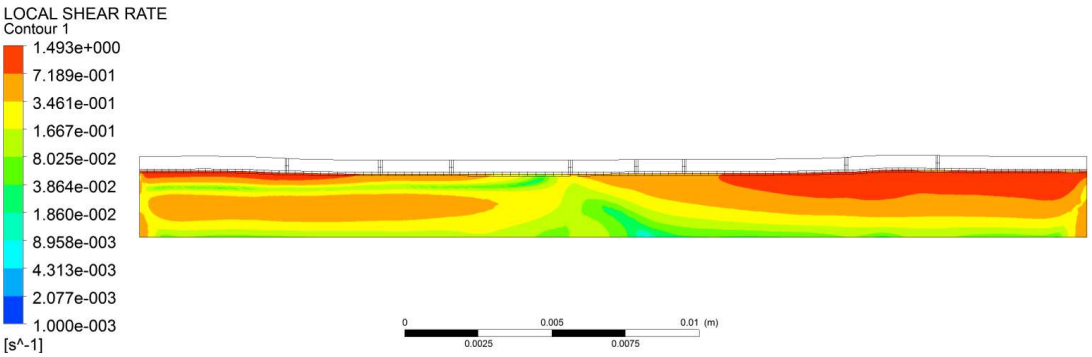

(a) Shear rates for water during a stretching motion. Time 4*s*.

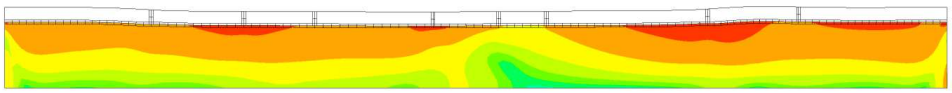

(b) Shear rates for honey during a stretching motion. Time 4*s*.

Fig. 8 Shear rates during a stretching motion. Time 4*s*.

than in the case of the oral motion. Figure 8 shows the shear rates observed during the motion at $4s$ for the water and honey like fluids respectively. The shear rates for the Bird-Carreau fluid were again similar to those for honey, and even smaller than for the oral motion. The shear rates appear more consistent between the three fluids. As was the case for the oral motion, the largest shear rates are generated at the intestinal wall. The likely cause of the difference in the magnitude of velocity and shear rates between the low and high viscous fluids is the relative strength of the wall motions. It was observed experimentally that the oral motion displaced points on the intestinal wall more and with higher velocity than the two other motions, the stretching and compression. This hypothesis is tested in a set of numerical experiments in Section 4.5.

4.3 Compression.

The streamlines, velocities, and shear rate profiles for the compression were found to be largely similar and of the same magnitude as the stretching motion profiles. We see zones of recirculation where fluid elements may transition from the center of the lumen to the wall. We also note that, as with the stretching motion, the fluid velocities are much less than in the oral case.

4.4 Mixing analysis.

The amount of stretching imposed by the fluid flow on differential material elements provide the basis to investigate and characterise the efficiency of advective mixing within the intestinal flow domain. In order to investigate the advective performance of macro-scale motions within different regions of the intestine, we analysed the average stretching values over the whole domain and three sub domains. If R is the radius of the tube, we define our three domains (over the entire length of the intestine) as $A = [0, R/3]$, $B = [R/3, 2R/3]$, $C = [2R/3, R]$. Here A is the subdomain including the center of the lumen ($r = 0$), and C is the subdomain including the intestinal wall ($r = R$).

4.4.1 Spatial distribution of stretching. Figures 9 - 11 are the average log stretching lengths for the three motions for the three fluids under study. The averages are taken over the whole domain, the upper domain C, the middle domain B, and the lower domain A. Regardless of the motility pattern, the average stretching increases with proximity to the wall and is lowest nearer the center of the lumen.

It should also be noted that viscosity affects the amount of stretching. In Figures 9 the water-like fluid flow led to levels of stretching one order of magnitude higher than the thicker honey or the guar-gum (noting the different scales). This is a direct result of the velocity gradients which developed in each flow (see Figure 4). Figures 10- 11 indicate that for the stretching and compression motions the stretching was of the same order of magnitude for the three rheologies investigated.

It is also noted that there exists a wider distribution of stretching values within the intestine in the case of the low viscous fluid. The plots for honey are much more uniform between the domains than those of water. This follows from Figure 4 (b) where the higher viscosity fluid is capable of transporting momentum further into the intestinal core, creating a more even flow profile throughout the intestine. Also of note is that the stretching motion and the compression are more uniform than the oral propagation, even for the low viscous fluid. This result is explained by the more chaotic behaviour that develops within the intestine for these motility patterns (Figure 7). It is also clear from the above graphs that the stretching values for the guar gum in each of the domains are very similar to those for honey, regardless of the type of motion.

Figure 12 displays on the same graph the average log stretching lengths averaged over the whole intestinal domain for the three motions for each fluid. It is apparent that the oral propagation creates the largest amount of stretching, and that low viscosity fluids creates more stretching. It is clear from this graph that guar gum is again behaving largely similar to honey. To investigate whether the amount of stretching increases with time, we will analyse the time average log stretching rates in the next sub-section.

4.4.2 Rate of stretching. In addition to the average (log) stretching length we also plot the time averaged log stretching. This will allow us to more clearly see the temporal evolution of the stretching field generated by the intestinal motion. Figure 13 plots the time averaged log stretching. It is clear that the amount of stretching generated by intestinal flows increases regardless of the motility pattern of the wall or the viscosity of the fluid. It is also obvious that the oral motion has the steepest trending gradient, indicating that this motion will produce the most stretching over time, particularly for low viscous fluids.

4.5 Impact of the strength of the intestinal motility.

A natural question arises when considering the results of the previous two sub-sections. Why does the oral motion produce more fluid stretching than the other two motions when it produces a highly ordered flow with little flow recirculations in comparison to the other motions? (see Figure 4 and Figure 7). To explain this observation, it is important to consider the strength of the motor activity of the intestinal wall for each of the motilities under study. Figure 14 displays the average absolute velocity of the intestinal wall over simulation time for the three motions. The oral motion has a max velocity $\approx 3\times$ that of the other two motions. Additionally, if the average wall velocity is calculated it is found that, in the case of the oral motion, the intestinal wall moved approximately six times faster than the other two motions. We believe that this accounts for

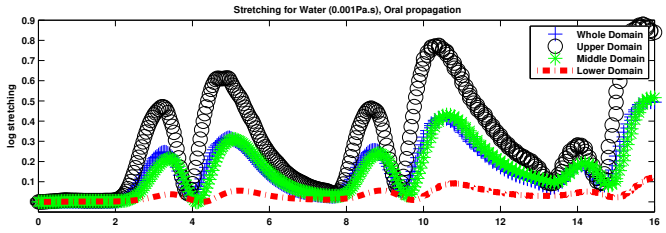

(a) log(stretching) during an oral motion for water.

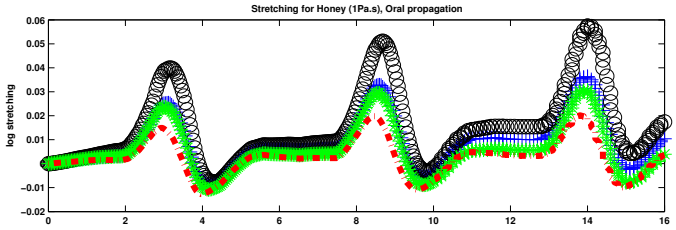

(b) log(stretching) during an oral motion for honey.

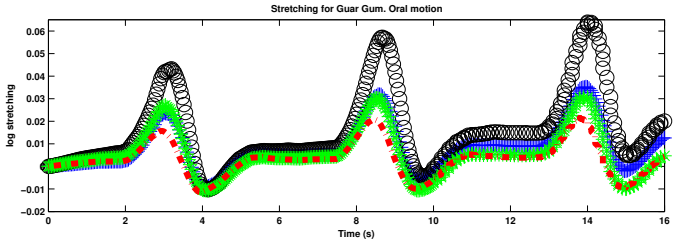

(c) log(stretching) during an oral motion for guar gum.

Fig. 9 log(stretching) during an oral motion.

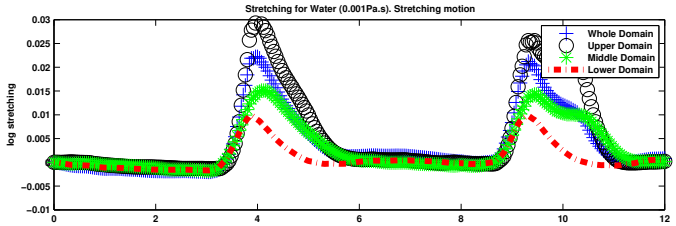

(a) log(stretching) during a stretching motion for water.

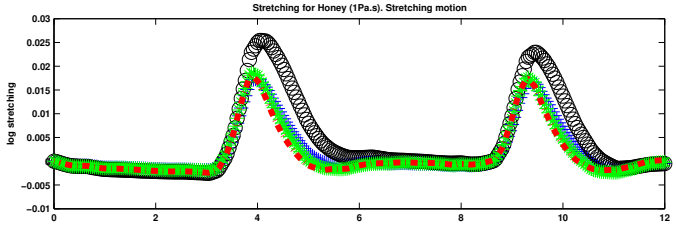

(b) log(stretching) during a stretching motion for honey.

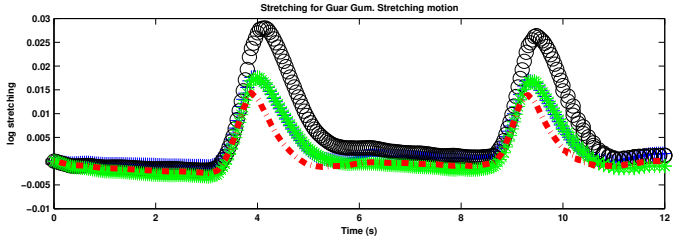

(c) log(stretching) during a stretching motion for guar gum.

Fig. 10 log(stretching) during a stretching motion.

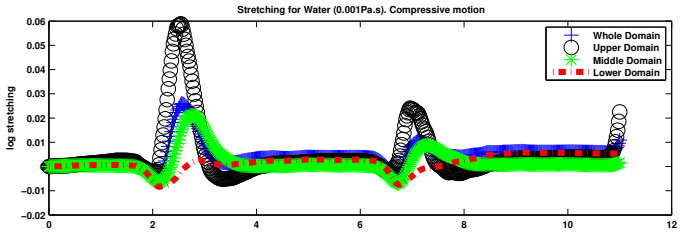

(a) log(stretching) during a compressive motion for water.

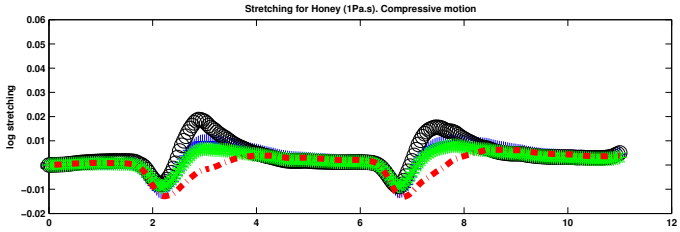

(b) log(stretching) during a compressive motion for honey.

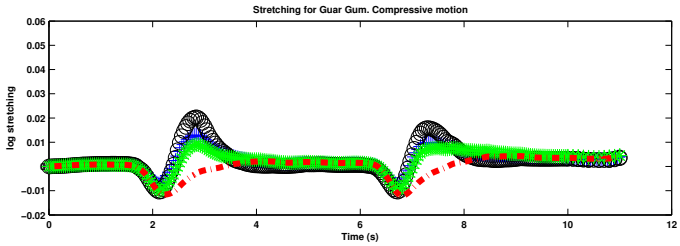

(c) log(stretching) during a compressive motion for guar gum.

Fig. 11 log(stretching) during a compressive motion.

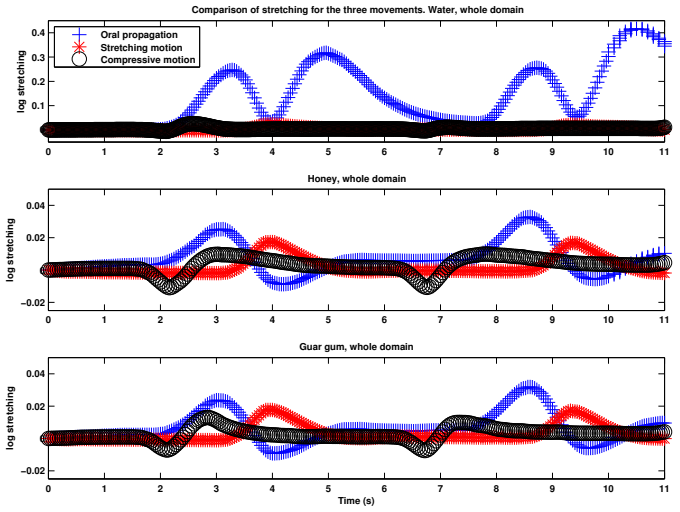

Fig. 12 Average log stretching over the whole domain for the three motions. Water (above), honey (middle), guar gum (bottom).

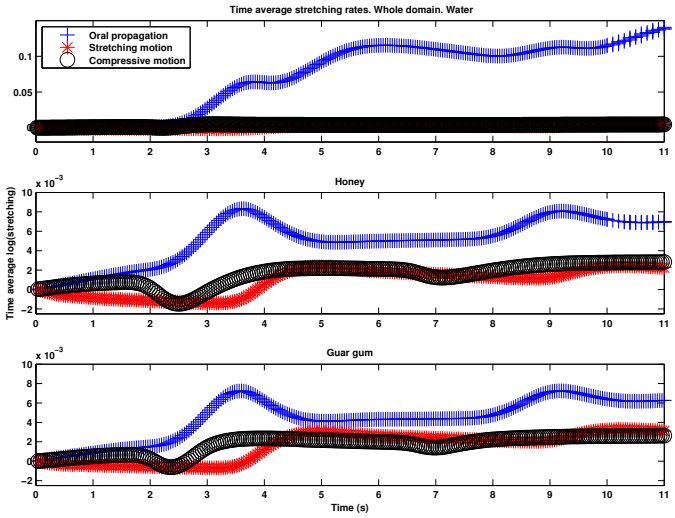

Fig. 13 Time averaged log stretching over the whole domain for the three motions. Water (above), honey (middle), guar gum (bottom).

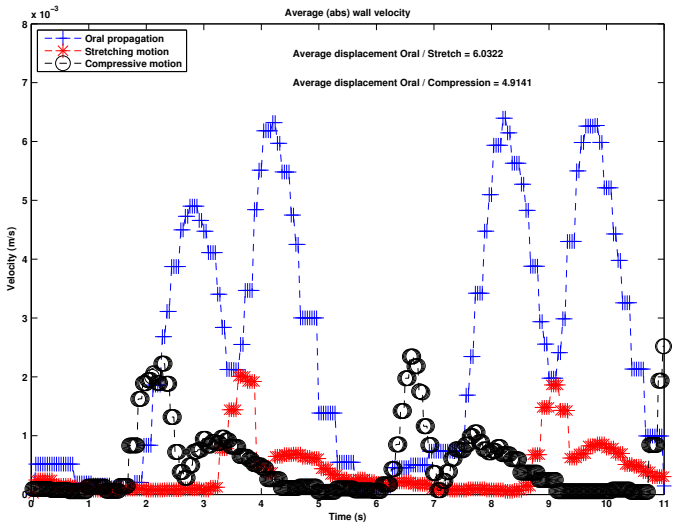

Fig. 14 Average wall velocity of each longitudinal motion.

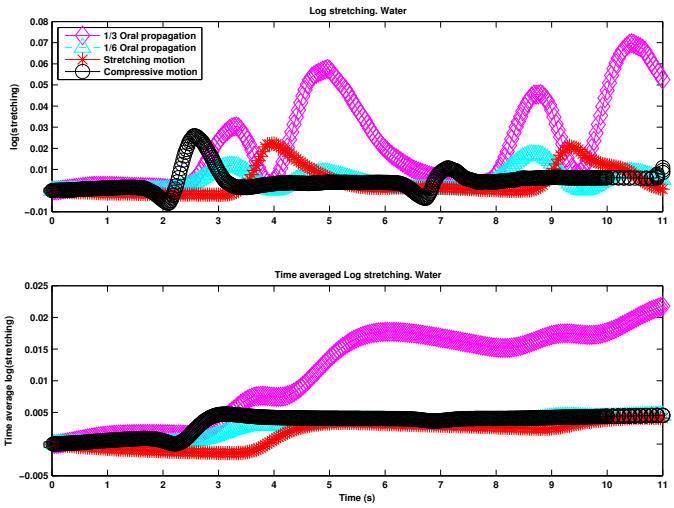

Fig. 15 The average (above) and time average (below) log stretching over the whole domain for water and for an oral motion of $1/3$ and $1/6$ strength the original. This is compared to the original stretching and compressive motions.

the enhanced mixing efficiency of the oral motility pattern. To test this hypothesis we repeated the numerical simulations for an oral motion with a third and a sixth the original strength. The timing of all contractions were kept constant (to account for the fact that the period of contractions are determined by the slow wave pacemaker frequency), only the velocity (and hence, displacement of the points on the intestinal wall) was reduced. Figure 15 shows the result of our trial simulation. The average of the log stretching is plotted for the stretching motion, the compression, and the two reduced strength oral motions. It is evident from the graphs that the oral motion which is reduced by a third is still larger than the stretching and compressive motions. However, the stretching for the oral motion which has been reduced by a sixth is now of the same (and in fact, slightly smaller) than the other two motions. This provides evidence that the strength of the wall motion in the oral case is the cause of higher stretching values. It is important to note that these motions were observed ex-vivo. It is unknown whether these motions exist in the rabbit in-vivo and if they do it is unknown if they are the same strength as was observed. We can conclude that if these motions are representative of those in-vivo then we expect longitudinal motions, in particular oral motions, to enhance the ability of the flow to advect nutrients and other intestinal contents in the small intestine.

5 Discussion.

The main goal of this work was to quantify the effect of three observed types of longitudinal motion for three fluids, both Newtonian and non-Newtonian, on mixing in the small intestine. Wang et al.[12] note that

> the enhancement of absorption by the MML (micro-mixing layer) in the presence of macro-scale transport is quite significant.

It seems reasonable then that flows with higher stretching values will engender absorption at the wall interface by increasing macro-scale shear, mixing, and transport of intestinal contents, and by exposing the mucosa to a greater fluid area as differential fluid elements are stretched and folded. The implicit hypothesis, that the stretching values are a proxy for absorption at the border brush zone, should be tested in a future work. It was found that the oral motion was the strongest of the three motions and subsequently produced the largest stretching of fluid elements. However, efficient mixing was highly dependent on distance from the border brush zone (wall region) of the intestine, particularly in the case of low viscous (water-like) fluids. In the case of a high-viscous fluid, the stretching was more uniform throughout the domain. This suggests that the efficiency of this motion in the advection of digestive secretions and nutrients along the wall but not necessarily in creating a good level of lumenal mixing across the intestine. The stretching motion and the compression generated a more uniform and slower flow with a more uniform distribution of stretching rates within the system. Results illustrated that these motions have a lesser ability to impart advection within the domain compared to the oral motion. The rheology of digesta was also found to have a significant effect on the dynamics and advective performance of the flow. Firstly, it was found that, for an oral motion, for a low viscous water-like fluid there existed a definite velocity gradient between the wall and the center of the lumen (Figure 4 (a)), whereas a high

viscous fluid like honey was able to flow in a more plug like fashion, as in Figure 4 (b). It was found that the shear rates generated during longitudinal motions in the small intestine were too low to significantly alter the apparent viscosity of the non-Newtonian fluid under study. The flow mainly behaved like a Newtonian fluid and had similar stretching values to the honey-like fluid. It remains to be seen if the shear rates generated by a circular contraction of the intestine (segmentation or a peristaltic wave) are of enough strength to alter the viscosity of non-Newtonian fluids significantly. The ability of stretching or compressive motions to promote advection is lesser than an oral motion, particularly in the case of water. The flow field generated by a stretching or compressive motion leads to a lower but more uniform distribution of stretching within the intestinal domain.

In Figure 15 the results of a test numerical experiment were presented. The oral motion was weakened by a factor of $1/3$ and then $1/6$ and the resulting stretching plotted. In the case of the $1/6$th reduction, it was found that the stretching length, compared with the stretching motion and compressive motion, were comparable. This lends evidence to the idea that, in the case of a low viscous fluid, the oral motion engendered greater advection than the other motions due to the intestinal wall moving at a higher velocity.

During this work it became clear that literature on the elastic properties of the intestine is widely variable, see Table 2. Wall properties will not have a significant effect on the results presented here as the deformation is controlled by the motion of selected markers. However, this fact warrants further attention in future work. Additionally, the small intestine has been shown to exhibit a viscoelastic type of response to imposed stresses[22]. It may be necessary to model the intestinal wall using such a model in future work.

The authors plan to simulate a segmentive contraction pattern in the same system and compare the resulting stretching lengths with the results obtained in this work. Additionally, we plan to simulate circular and longitudinal motions simultaneously, as was observed in some (as yet) unpublished experiments. This should quantify how large an effect longitudinal motions have on mixing in the intestine. The intestinal wall was assumed smooth in this work. Special attention should be given to the effect of roughness of the wall and the presence of a slip condition (due to villi and mucous effects). Finally, it is noteworthy that our current work focuses on bulk mixing in the whole organ, and can be treated as a macro-scale model which does not account for micro-scale effects.

References

1 R. G. Lentle and P. W. Janssen, *The physical processes of digestion*, Springer, 2011.

2 S. K. Sarna, *American Journal of Physiology-Gastrointestinal and Liver Physiology*, 1993, **265**, G156–G164.

3 L. Thuneberg and S. Peters, *The Anatomical Record*, 2001, **262**, 110–124.

4 E. O. Macagno and J. Christensen, *Annual Review of Fluid Mechanics*, 1980, **12**, 139–158.

5 R. Lentle, C. De Loubens, C. Hulls, P. Janssen, M. Golding and J. Chambers, *Neurogastroenterology & Motility*, 2012, **24**, 686–e298.

6 W. J. Lammers, *American Journal of Physiology-Gastrointestinal and Liver Physiology*, 2005, **289**, G898–G903.

7 J. Melville, E. Macagno and J. Christensen, *American Journal of Physiology–Legacy Content*, 1975, **228**, 1887–1892.

8 C. de Loubens, R. G. Lentle, R. J. Love, C. Hulls and P. W. Janssen, *Journal of The Royal Society Interface*, 2013, **10**, 1–12.

9 W. J. Lammers, L. Ver Donck, J. A. Schuurkes and B. Stephen, *American Journal of Physiology-Gastrointestinal and Liver Physiology*, 2003, **285**, G1014–G1027.

10 *Videos of experimentally observed longitudinal motions of the rabbit small intestine.*, 2014, http://tinyurl.com/qazbsgv.

11 R. Lentle, P. Janssen, C. DeLoubens, Y. Lim, C. Hulls and P. Chambers, *Neurogastroenterology & Motility*, 2013, **25**, 881–e700.

12 Y. Wang, J. G. Brasseur, G. G. Banco, A. G. Webb, A. C. Ailiani and T. Neuberger, *Philosophical Transactions of the Royal Society A: Mathematical, Physical and Engineering Sciences*, 2010, **368**, 2863–2880.

13 R. G. Lentle, P. W. Janssen, P. Asvarujanon, P. Chambers, K. J. Stafford and Y. Hemar, *Journal of Comparative Physiology B*, 2007, **177**, 543–556.

14 J. Zhao, D. Liao, J. Yang and H. Gregersen, *Journal of biomechanics*, 2011, **44**, 2077–2082.

15 D. Liao, J. Yang, J. Zhao, Y. Zeng, L. Vinter-Jensen and H. Gregersen, *Medical engineering & physics*, 2003, **25**, 413–418.

16 J. Ohayon, *Comptes Rendus de l'Académie des Sciences-Series IIB-Mechanics-Physics-Chemistry-Astronomy*, 1997, **324**, 179–187.

17 X. Chai, M. van Herk, J. B. van de Kamer, M. C. Hulshof, P. Remeijer, H. T. Lotz and A. Bel, *Medical physics*, 2011, **38**, 142.

18 M. Velec, J. L. Moseley, C. L. Eccles, T. Craig, M. B. Sharpe, L. A. Dawson and K. K. Brock, *International Journal of Radiation Oncology* Biology* Physics*, 2011, **80**, 265–272.

19 B. Hari, S. Bakalis and P. Fryer, *Proceedings of the 2012 COMSOL Conference*, 2012.

20 E. J. Chen, J. Novakofski, W. K. Jenkins and W. D. O'Brien Jr, *Ultrasonics, Ferroelectrics and Frequency Control, IEEE Transactions on*, 1996, **43**, 191–194.

21 J. M. Ottino, *The kinematics of mixing: stretching, chaos, and transport*, Cambridge University Press, 1989, vol. 3.

22 H. Gregersen, J. Emery and A. McCulloch, *Annals of biomedical engineering*, 1998, **26**, 850–858.